

Conformational Transition of Membrane-Associated Terminally Acylated HIV-1 Nef

Bulent Akgun,^{1,2,3} Sushil Satija,¹ Hirsh Nanda,^{1,2} Gregory F. Pirrone,⁴ Xiaomeng Shi,⁴ John R. Engen,⁴ and Michael S. Kent^{5,*}

¹National Institute of Standards and Technology, Gaithersburg, MD 20899, USA

²Department of Materials Science and Engineering, University of Maryland, College Park, MD 20742, USA

³Department of Chemistry, Boğaziçi University, Bebek 34342, Istanbul, Turkey

⁴Department of Chemistry and Chemical Biology, Northeastern University, Boston, MA 02115, USA

⁵Sandia National Laboratories, Albuquerque, NM 87123, USA

*Correspondence: mskent@sandia.gov

<http://dx.doi.org/10.1016/j.str.2013.08.008>

SUMMARY

Many proteins are posttranslationally modified by acylation targeting them to lipid membranes. While methods such as X-ray crystallography and nuclear magnetic resonance are available to determine the structure of folded proteins in solution, the precise position of folded domains relative to a membrane remains largely unknown. We used neutron and X-ray reflection methods to measure the displacement of the core domain of HIV Nef from lipid membranes upon insertion of the N-terminal myristate group. Nef is one of several HIV-1 accessory proteins and an essential factor in AIDS progression. Upon insertion of the myristate and residues from the N-terminal arm, Nef transitions from a closed-to-open conformation that positions the core domain 70 Å from the lipid headgroups. This work rules out previous speculation that the Nef core remains closely associated with the membrane to optimize interactions with the cytoplasmic domain of MHC-1.

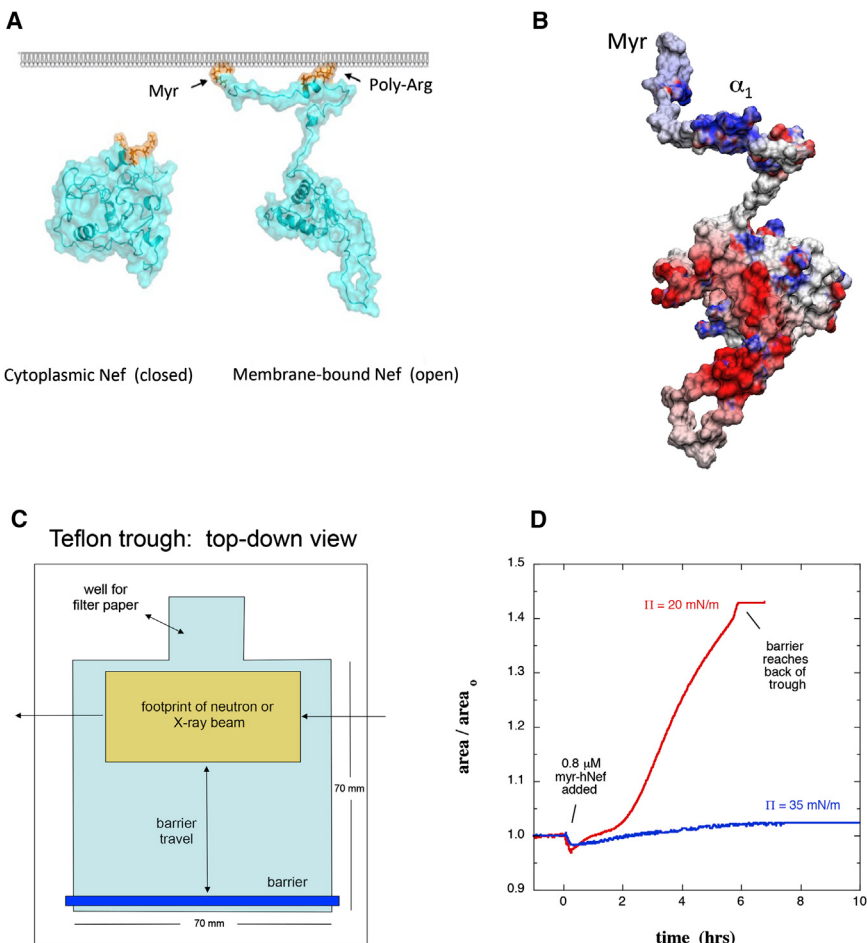
INTRODUCTION

There is abundant evidence that enzyme activity or protein-protein interactions can depend upon association with lipid membranes. The positioning of proteins and protein motifs relative to either the membrane or to other membrane-bound proteins is, for some proteins, critical and may depend on conformational changes induced upon membrane association (Kim et al., 2009; Osterhout et al., 2003; Schlessinger, 2000; Subramanian et al., 2006; Xue et al., 2004; Zha et al., 2000). Lipid modification serves to target many proteins to specific membranes or submembrane locations. Hundreds of proteins are modified with covalently bound lipid groups, the most common of which are fatty acids, isoprenoids, and glycosylphosphatidylinositol anchors (Farazi et al., 2001; Jeromin et al., 2004; Perinpanayagam et al., 2013; Resh, 2006; Steinhauer and Treisman, 2009). Many of these proteins are involved in signaling and require membrane association to signal efficiently. In addition to intracellular membrane location, the structure adopted by pro-

teins at membranes is also critical for certain functions. As an example, myristoyl or farnesyl switch mechanisms are known for more than a dozen proteins, with Arf GTPase being a hallmark example (Goldberg, 1998; Resh, 2006). These mechanisms cause proteins to switch between conformational states in which the myristoyl or farnesyl moiety is either sequestered or exposed and can promote membrane binding (Ames et al., 1996; Goldberg, 1998), facilitate release from the membrane-bound state (Ames et al., 1996; Goldberg, 1998; Hantschel et al., 2003; Matsubara et al., 2004; McLaughlin and Aderem, 1995; Resh, 2006), and regulate protein-protein interactions (Hantschel et al., 2003; Matsubara et al., 2004).

Despite the obvious importance of acylated proteins in biology (e.g., kinases and phosphatases [Kim et al., 2009; Resh, 2006; Schlessinger, 2000], G proteins [Resh, 2006], GPCRs [Resh, 2006], morphogens [Steinhauer and Treisman, 2009], neuronal calcium sensors [Jeromin et al., 2004], pro- and anti-apoptotic proteins [Perinpanayagam et al., 2013]), standard approaches for studying their structure at membranes are neither adequate nor appropriate. In addition, understanding signaling mechanisms involving these proteins at the molecular level and developing pharmaceutical interventions have been limited by the absence of structural detail for these proteins in the membrane-bound state. Many structural studies of membrane-associated proteins have consisted of crystallization of soluble proteins with and without bound ligand or in complex with other proteins but in the absence of a membrane (Ames et al., 1996; Flaherty et al., 1993; Goldberg, 1998; Matsubara et al., 2004). Nuclear magnetic resonance (NMR), electron paramagnetic resonance (EPR), fluorescence resonance energy transfer (FRET), Fourier transform infrared-attenuated total reflection spectroscopy (FTIR-ATR), and other methods can be applied to provide some structural details for proteins associated with membranes or membrane mimics, but do not give the full residue distribution with respect to the membrane.

A case in which it is essential to define the structural details of a protein at the membrane is the Nef protein from HIV-1. Nef is one of several HIV-1 accessory proteins and is essential for AIDS progression (Baur, 2004; Das and Jameel, 2005). Nef is expressed in high concentrations shortly after viral infection (Klotman et al., 1991) and is required for achieving and maintaining high viral loads in vivo (Goldsmit et al., 1995). Nef lacks catalytic activity but instead realizes its functions by interacting with host proteins—more than 30 proteins that interact with Nef have

**Figure 1. Hypothetical Molecular Models of Nef in Solution and Bound to a Membrane**

(A) Left: Nef (cyan) adopts a tightly closed conformation in the cytoplasm. Right: Nef interacts with lipid bilayers via an N-terminal myristate group and poly-Arg cluster (orange). The open Nef model was adapted from Aruld and Baur (Aruld and Baur, 2001).

(B) Distribution of surface charge on myr-Nef displayed from -8 (red) to $+8$ (blue) k_bT (open form model of Geyer and Peterlin, 2001).

(C) Diagram (top-down view) of the trough used in the NR (XR) measurements. The beam footprint in the NR (XR) studies was 25 mm (10 mm).

(D) Change in surface area upon binding of myr-Nef ($0.83 \mu\text{M}$) at 20 mN/m and 35 mN/m . Area_0 is the lipid-containing surface area prior to injecting protein.

been identified (Aruld and Baur, 2001; Baur, 2004; Renkema and Saksela, 2000). Nef exists in both membrane-associated and cytosolic fractions (Coates et al., 1997) and shuttling may occur between the cytosolic fractions and the membrane-associated form (Figure 1A; Bentham et al., 2006). Membrane association is achieved by an N-terminal myristylation essential for the virus *in vivo* (Harris, 1995) as well as a cluster of basic residues (17–22) within the N-terminal arm (Figure 1B; Bentham et al., 2006; Curtain et al., 1998; Gerlach et al., 2010). The myristylation motif (residues 2–7) is essential and highly conserved in Nef alleles from both laboratory HIV-1 strains and in primary isolates from AIDS patients (Geyer et al., 1999). Deletion of the myristate (myr) group from Nef dramatically reduces infectivity (Goldsmith et al., 1995), cripples downregulation of CD4 and MHC-I (Goldsmith et al., 1995; Peng and Robert-Guroff, 2001), and prevents formation of an AIDS-like disease in mice transfected with Nef (Hanna et al., 2004). Both the myr group and the basic cluster are required for Nef virion incorporation (Welker et al., 1998). Nef residues 5–22 form an amphipathic helix with hydrophobic residues Trp5, Trp13, Ile16, and Met20 located on one side of the helix. Gerlach and colleagues reported significantly decreased binding affinity to lipid membranes and impaired helix formation upon mutation of Trp5 and Trp 13 (Gerlach et al., 2010).

It has been postulated that Nef undergoes a transition from a solution conformation to a membrane-associated conformation (Figure 1A), and this conformational rearrangement enables membrane-associated Nef to interact with host proteins (Aruld and Baur, 2001; Geyer and Peterlin, 2001; Jia et al., 2012; Raney et al., 2007). In particular, it has been suggested that insertion of the N-terminal arm and subsequent displacement of the core domain from the lipid membrane will expose binding sites on the core, facilitating interaction with host proteins (Aruld and Baur, 2001). On the other hand, based on the crystal structure of Nef with the cytoplasmic tail of MHC-I, others have suggested that association of Trp13 and Met20 on the N-terminal arm with the core domain persists upon membrane binding, and that this positions the Nef core close to the membrane for optimal interaction with the cytoplasmic domain of the MHC-I receptor (Jia et al., 2012). Others have proposed that association of the core domain of Nef with negatively charged membranes through its basic surface (Figure 1B) orients Nef to provide optimal exposure of the dileucine sorting motif in the flexible loop (residues 152–184) that mediates interactions with adaptor protein complexes (Horenkamp et al., 2011). Nef is known to upregulate several but not all Src family kinases through interaction with their SH3 domains (Narute and Smithgall, 2012), critical to many downstream functions. These kinases are also bound to the membrane through N-terminal acylation, and positioning of the Nef core domain relative to the SH3 domains may play a role in the varying binding affinities. Despite the vital importance to the pathogenicity of Nef, there is no information regarding the position of the core of Nef upon membrane association due to the limitations of current structural methods.

FRET has been used to detect membrane binding and insertion of Nef by Gerlach and colleagues (Gerlach et al., 2010). From kinetic studies, they identified two processes and

proposed a model for the stages of interaction, but structural information for full Nef was absent from their model. Prior structural work, while providing critical insights, has been confined to solution-based analyses even though membrane association is critical for Nef function (Arold et al., 1997; Grzesiek et al., 1996, 1997; Jia et al., 2012; Jung et al., 2011; Lee et al., 1996). While methods such as circular dichroism (Gerlach et al., 2010) and FTIR-ATR are available to assay changes in secondary structure upon membrane binding, full global conformational characterization including distances of motifs relative to the membrane are not provided by these methods.

In the current work, neutron and X-ray reflectometry (NR and XR) were used to resolve conformational changes in myristoylated Nef (myr-Nef) upon membrane insertion. Reflectivity is one of very few methods that can resolve structural details of membrane-associated proteins in physiological conditions and may be unique in the ability to directly resolve details of the full membrane-bound protein structure, in contrast to techniques that probe only labeled residues or secondary structural elements. NR and XR involve measuring the ratio of reflected to incident intensity as a function of momentum transfer $q_z = 4\pi \sin\theta/\lambda$, where θ is the angle of incidence with respect to the plane of the membrane and λ is the wavelength (Penfold and Thomas, 1990). The form of this curve is determined by the in-plane averaged scattering length density (SLD) profile normal to the surface. The neutron SLD is determined by the properties of the nuclei present, whereas the X-ray SLD is determined by the electronic properties. In both cases, the SLD is directly related to the atomic composition and the density. Therefore, for a protein bound to a planar lipid membrane, NR and XR determine the in-plane averaged distribution of amino acid residues normal to the membrane in a complementary way. Typically, XR covers a q_z range that extends to higher values than achievable by NR, and hence XR provides greater insight into the effect of myr-Nef binding and insertion on the structure of the lipid layer. The contrast for the protein in buffer with XR is comparable to, but slightly weaker than, that for NR with protonated myr-Nef, yet is still sufficiently high to resolve large changes in the residue profile. The NR contrast for deuterium-enriched myr-Nef in buffer is substantially greater than that with XR and NR with protonated myr-Nef. Langmuir monolayers and lipid bilayers supported on a solid substrate can both be used as model lipid membranes in NR/XR studies of membrane-bound proteins (Chen et al., 2009; Datta et al., 2011; Kent et al., 2010; McGillivray et al., 2009; Nanda et al., 2010; Shenoy et al., 2012). For biophysical studies, Langmuir monolayers provide an advantage in that the membrane pressure can be controlled and are especially suitable when proteins are known to insert into only the outer leaflet of lipid bilayers.

Myr-Nef (strain SF2) was injected underneath a Langmuir monolayer of deuterated dipalmitoylphosphatidylglycerol (dDPPG) and its conformation was resolved by NR and XR as a function of membrane conditions. The structural details of membrane-bound Nef as a function of solution concentration, membrane pressure, and Nef coverage are described below. The data demonstrate a large conformational change from a closed to an open form that displaces the Nef core domain 70 Å from the lipid headgroups upon insertion of the myristate group and residues of the N-terminal arm. This large confor-

tional change is likely to affect its ability to interact with host proteins by exposing binding motifs on the core domain or by optimally positioning the core domain for interaction with motifs of membrane-associated host proteins.

RESULTS

The NR and XR data in this study indicated that soon after myr-Nef was introduced underneath the lipid membrane, a process of insertion into the membrane occurred accompanied by a large conformational transition. Because the affinity of myr-Nef for lipid membranes increases with the percentage of negatively-charged lipid, lipid monolayers composed entirely of dDPPG were used in most of this work to maximize the binding affinity, although some experiments were performed using a more biologically relevant ratio of 30% negatively charged lipid to 70% neutral lipid. When myr-Nef was circulated underneath the monolayer, insertion of myr-Nef into the membrane was evident by the backward movement of the trough barrier maintaining the monolayer pressure (increase in surface area at fixed number of lipid molecules, see Figures 1C and 1D and described in more detail in the [Experimental Procedures](#)). The insertion was dependent on the membrane pressure, with insertion readily occurring at 25 mN/m and lower but not at 35 mN/m (Figure 1D, and see also below). Due to the larger area occupied by the core domain relative to that of the myristate group, insertion of the myristate moiety alone can account for an increase in surface area of at most 5%; increases in surface area greater than 5% therefore indicate insertion of residues of the protein in addition to the myristate group. Others have reported membrane insertion and evidence for formation of an amphipathic helix within the N-terminal 27 residues of Nef upon association to lipid membranes (Gerlach et al., 2010). Upon insertion, myr-Nef remained associated with the membrane throughout extensive exchange of the subphase underneath the surface layer to remove noninserted, loosely bound myr-Nef. On the other hand, when insertion was inhibited (35 mN/m), membrane-associated myr-Nef was readily removed upon subphase exchange. The rate and extent of insertion of residues varied when membrane pressure was held constant and the concentration of myr-Nef was changed, and vice versa.

To interrogate the membrane-associated conformation of Nef, several NR studies were performed at a fixed membrane surface pressure of 30 mN/m and variable myr-Nef concentration, shown in Figure 2 (NR data in panel a and the SLD profiles resulting from the fitting analysis in panel b). At a myr-Nef concentration of 0.25 μM a fractional surface coverage (f) of 0.21 resulted (the fractional surface coverage is arbitrarily defined such that when $f = 1.0$, the core domains of all Nef molecules would just come into contact with one another in the open conformation shown in Figure 2B), little change in surface area occurred, and a form of Nef that was compact with the core domain adjacent to the lipid headgroups (hereafter referred to as the closed form) was observed. At a myr-Nef concentration of 1.0 μM, the fractional coverage was 0.62, a large increase in area occurred (25%), and a completely different conformation was observed for myr-Nef. For this conformational state (hereafter referred to as the open form) the core domain was displaced ~70 Å below the lipid headgroups (Figure 2B).

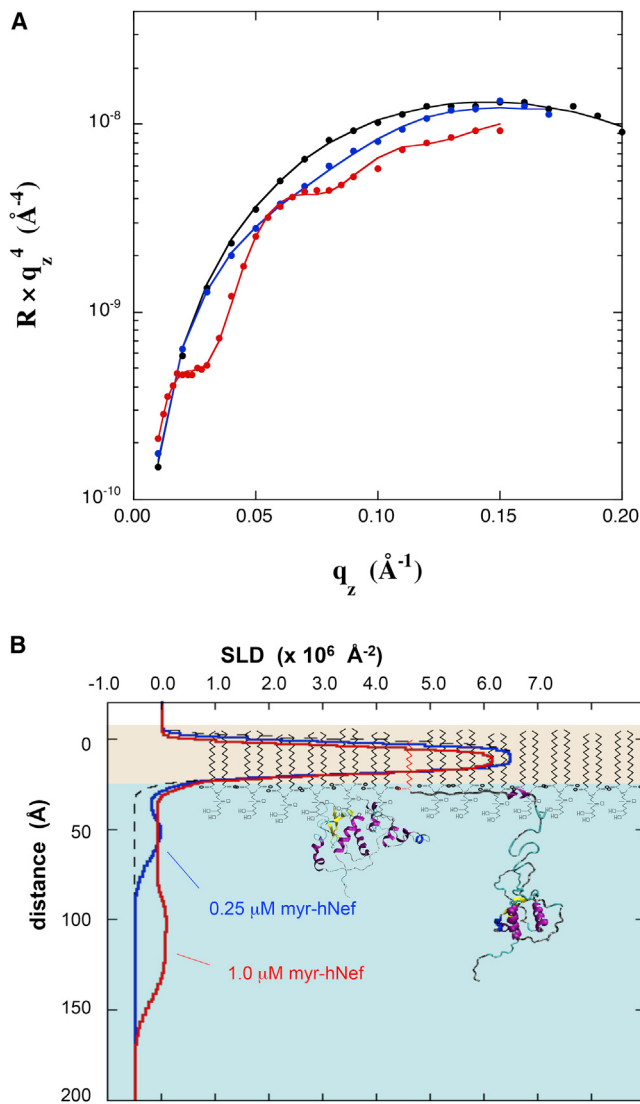


Figure 2. NR Results for myr-Nef Adsorbed to a dDPPG Monolayer at 30 mN/m

(A) NR data for a dDPPG monolayer at 30 mN/m on Tris-buffered H₂O subphase (black) and with myr-Nef adsorbed from solutions at 0.25 μM (blue) and at 1.0 μM (red). Error bars at the highest q_z values are the size of the data points and denote the uncertainty in the counting statistics.

(B) SLD profiles corresponding to the data in (A). The molecular models of dDPPG and of Nef are not drawn precisely to scale but were scaled to coincide approximately with the corresponding features in the SLD profiles. See also Figure S1.

Further XR and NR studies were performed in which insertion and Nef conformation were controlled by adjusting the surface pressure of the lipid membrane. XR (Figures 3 and 4) and surface area data (Figure 1D) both indicate little insertion of residues at 35 mN/m, but substantial insertion of residues at 20 mN/m. In the XR data, the conformation of adsorbed protein is evidenced by the variation at low q_z (expanded in Figures 3B and 4B). In the low q_z region the XR curves show distinctly different patterns, and hence indicate different conformations of myr-Nef (0.83 μM), at the two membrane pressures. As shown in the

electron density profiles (Figures 3C and 4C) the core domain of myr-Nef was directly adjacent to the lipid headgroups at 35 mN/m, but was displaced 70 Å below the lipid headgroups at 20 mN/m, similar to the profile for 1 μM myr-Nef in Figure 2. At higher q_z the XR curves primarily reflect the structure of the dDPPG monolayer. In particular, the minimum in the data prior to myr-Nef addition indicates the thickness of the dDPPG layer. At 20 mN/m (Figure 3A), the minimum shifted from 0.28 Å⁻¹ to 0.33 Å⁻¹ after injecting myr-Nef. This shift in the minimum to higher q_z indicates that the thickness of the lipid layer decreased by 4 Å, consistent with tilting of the tails upon insertion of Nef residues. This is another indication of insertion of Nef residues into the lipid layer. At 35 mN/m (Figure 4A), the minimum was unchanged after injecting myr-Nef. Insertion of residues into the membrane and the open extended form of Nef was also observed at 25 mN/m (Figure S2 available online) and again for adsorption to 70/30 dDPPC/dDPPG membranes at 20 mN/m (Figure 5). Others have shown that myr-Nef only binds with high affinity to membranes containing at least 30% negatively charged lipids (Gerlach et al., 2010). The XR measurements are described further in the Supplemental Information.

Deuterium enrichment of the protein being analyzed in NR substantially increases the SLD contrast, allowing for higher resolution data and more precise fitting with molecular models. Myr-Nef in which 80% of the nonexchangeable hydrogen atoms were replaced by deuterium (myr-dNef) was prepared. Figure 6A compares the NR data for a monolayer of dDPPG at 35 mN/m on H₂O buffer compared with a scan after adsorption of myr-dNef. In this case, 0.5 μM myr-dNef was incubated against the monolayer for 8 hr and then the concentration was increased to 1.0 μM for 1 hr, at which point adsorption had slowed dramatically and a full scan was collected. The fractional coverage was 0.15. The best-fit SLD profile using a free-form slab model is shown in Figure 6B. The profile band indicates that the core domain lies directly against the lipid headgroups with an uncertainty of ± 5 Å.

The measurement was repeated for a monolayer of dDPPG at 20 mN/m, formed initially by spreading to a pressure of ~10 mN/m and then compressing to 20 mN/m. Myr-dNef (0.28 μM) was injected under the monolayer and a scan initiated 4 hr later (Figure 7A). A large increase in area resulted, similar to that seen for myr-hNef (Figure 1D), indicating substantial insertion of residues into the lipid membrane. The fractional coverage was 0.61. Relative to the NR data for myr-Nef in Figure 2A, a larger change was observed that allowed a much more refined model to be generated. The best-fit SLD profile using a free form slab model is shown in Figure 7B. The red/black profile band contains a broad maximum, indicating the core domain, again displaced roughly 70 Å from the lipid headgroups. Clearly, in the open conformation of Nef, as now derived from multiple NR and XR experiments, the bulk of Nef does not reside next to the membrane but rather is significantly displaced.

Further analysis was performed using molecular models of Nef in which the fractional area coverage and the position of the core domain normal to the membrane were adjusted as free parameters during fitting. As prior work by others indicated that, in addition to the myristate group, a cluster of basic residues within the N-terminal arm (17–22) interacts with negatively-charged lipid membranes to facilitate Nef adsorption

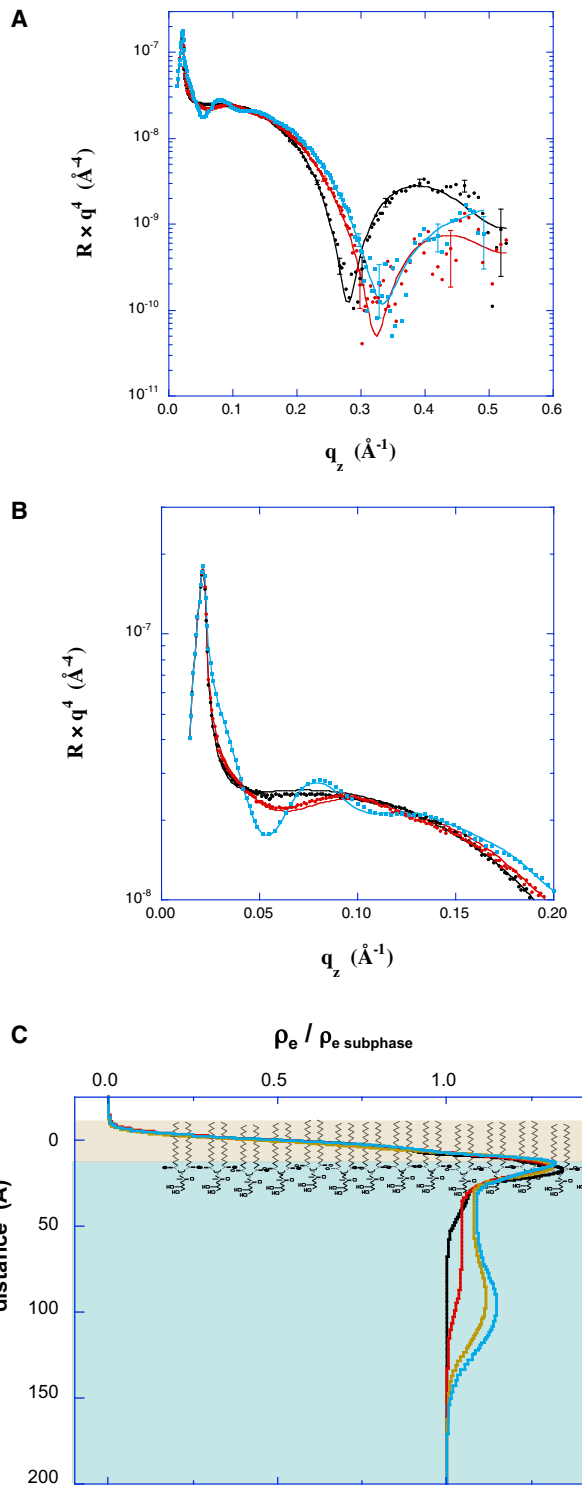


Figure 3. XR Results for myr-Nef Adsorbed to a dDPPG Monolayer at 20 mN/m

(A) XR data for a dDPPG monolayer at 20 mN/m (black) and scans initiated 2 hr (red) and 16 hr (cyan) after addition of myr-Nef at 0.83 μ M.
 (B) Expanded view of the XR data in (A) showing the low q_z region.
 (C) Electron density profiles corresponding to XR data in (A). Also included is the profile for a scan initiated 14 hr after the addition of myr-Nef (yellow).
 See also Figure S2.

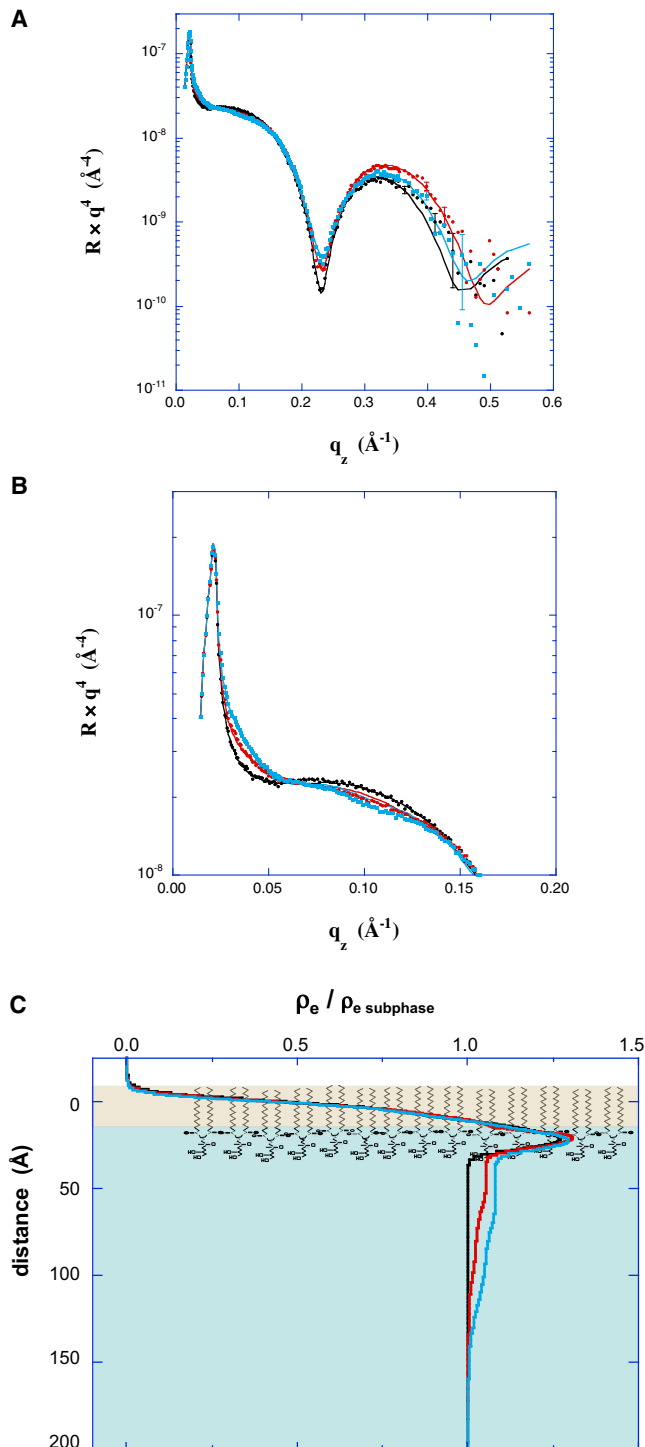


Figure 4. XR Results for myr-Nef Adsorbed to a dDPPG Monolayer at 35 mN/m

(A) XR data for a dDPPG monolayer at 35 mN/m (black) and scans initiated 4 hr (red) and 6 hr (cyan) after addition of myr-Nef at 0.83 μ M.
 (B) Expanded view of the XR data in (A) showing the low q_z region.
 (C) Electron density profiles corresponding to XR data in (A).

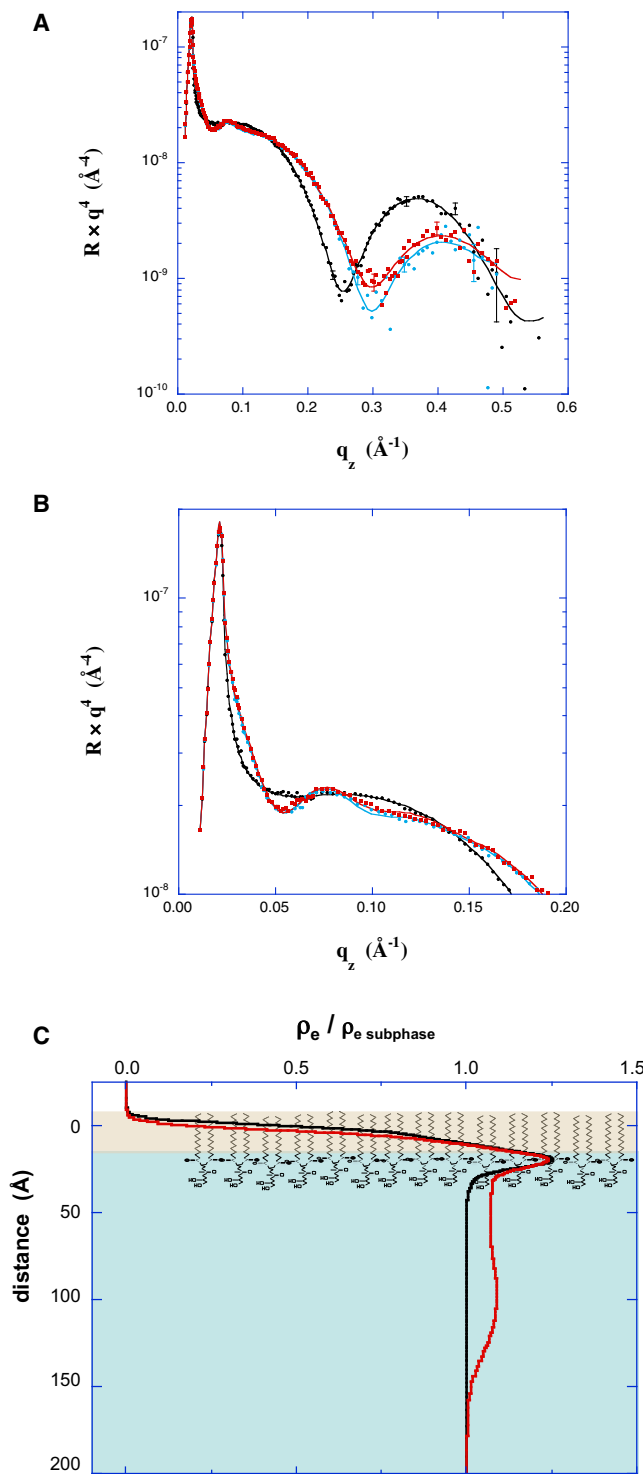


Figure 5. XR Results for myr-Nef Adsorbed to a 70/30 dDPPC/dDPPG Monolayer at 20 mN/m

(A) XR data for a 70/30 dDPPC/dDPPG monolayer at 20 mN/m (black) compared with a scan collected 22 hr after injecting 0.87 μM myr-Nef (cyan) and a scan collected after exchanging the subphase with buffer (red). (B) Expanded view of the XR data in (A) showing the low q_z region. (C) Electron density profiles corresponding to XR data in (A).

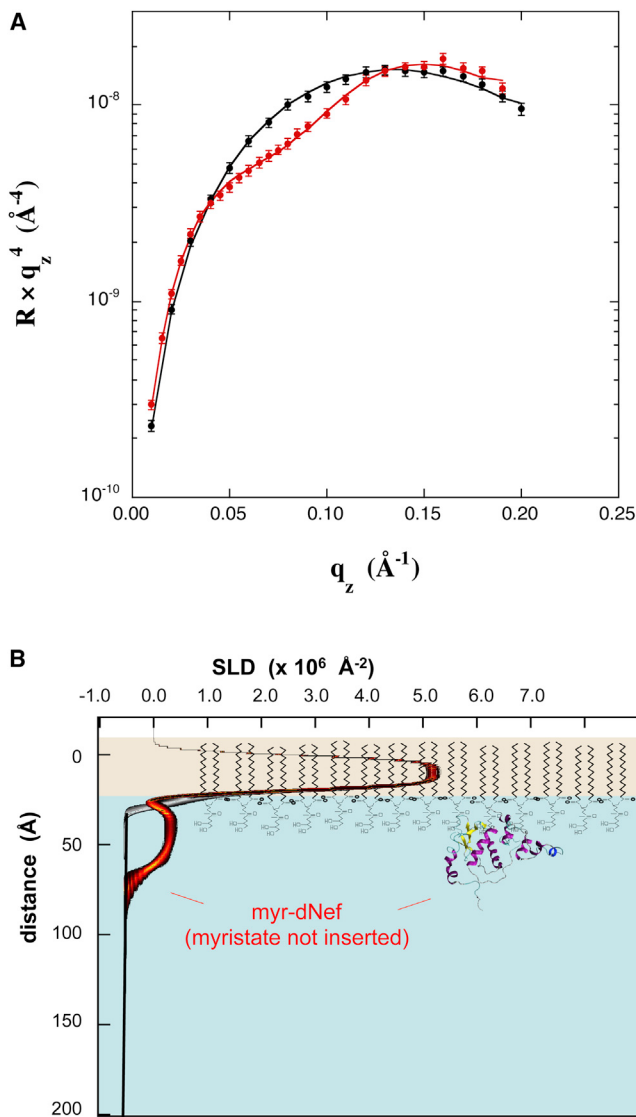


Figure 6. NR Results for myr-dNef Adsorbed to a dDPPG Monolayer at 35 mN/m

(A) NR data for a dDPPG monolayer at 35 mN/m on Tris-buffered H_2O subphase (black) and with bound myr-dNef adsorbed from solution at 1.0 μM (red). Best fit is shown using a free-form slab model.

(B) SLD profiles corresponding to the best-fits in (A). The black/gray and red/black bands correspond to the best-fit profiles for dDPPG alone and dDPPG with bound myr-dNef, respectively, with uncertainty limits using a free-form slab model. The molecular models of dDPPG and of Nef are not drawn precisely to scale but were scaled to coincide approximately with the corresponding features in the SLD profiles.

(Gerlach et al., 2010), only molecular models in which residues 2–22 resided on or within the lipid headgroups were considered. Molecular structures in which the core domain was located at varying distances from residue 22 were examined. In these calculations, a single orientation of the core domain was chosen arbitrarily, because it is not possible to resolve the distribution of core domain orientation from the present NR data. The structure giving the best agreement with the data is shown in Figure 7B (blue line), where the core domain is separated from residue 22

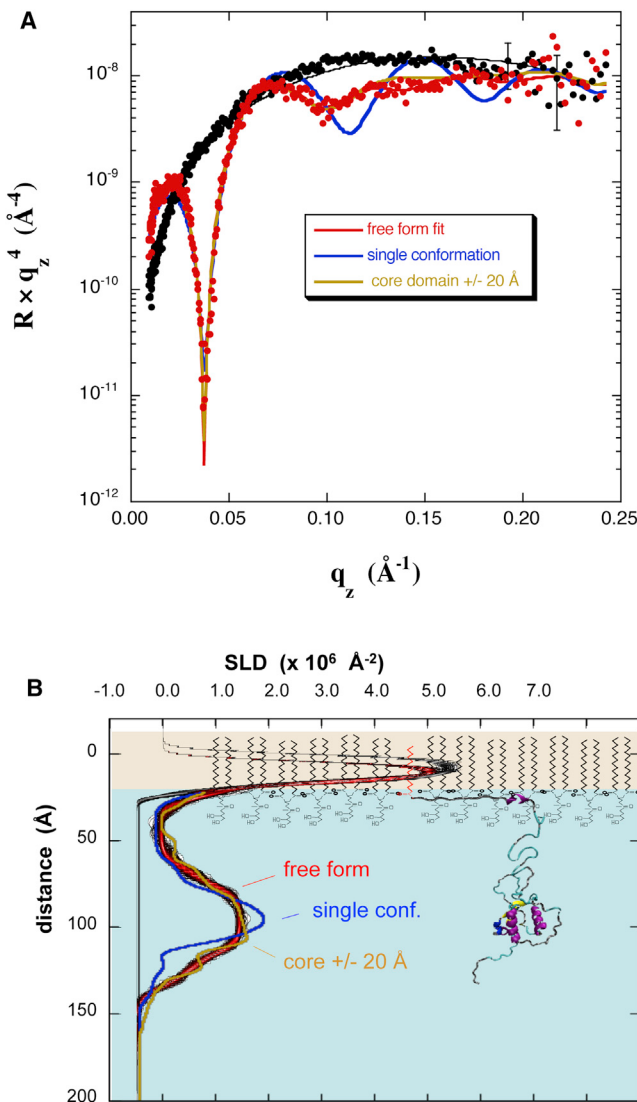


Figure 7. NR Results for myr-dNef Adsorbed to a dDPPG Monolayer at 20 mN/m

(A) NR data for a dDPPG monolayer at 20 mN/m on Tris-buffered H₂O subphase (black) and with bound myr-dNef adsorbed from solution at 0.28 μM (red). Best fits are shown using a free-form slab model (red), a model of Nef with residues 2–22 located in the membrane (blue), and an ensemble of three Nef structures in which the core domain distance from the membrane was adjusted $\pm 20 \text{ Å}$ relative to that of the structure shown in (B; yellow).

(B) SLD profiles corresponding to the best fits in (A). The red/black band corresponds to the best-fit profile with uncertainty limits using a free form slab model. The other curves have the same color coding as in (A). The molecular model of Nef used in the SLD calculations is shown scaled such that the core domain coincides with the peak in the SLD profile. The lipids are not drawn precisely to scale.

See also Figure S3.

by 70 Å and the peak in SLD corresponding to residues 2–22 is located within the lipid headgroups. The fit to the data, however, is poor because the best-fit curve shown in Figure 7A (blue line) contains greater oscillations at higher q_z values than are present in the data, and the calculated SLD profile contains a maximum that is considerably narrower than that of the profile from the

free-form fit. This result indicates that the core domains are distributed over a range of depth. Combining the myr-dNef structure shown in Figure 7B with structures in which the core domain is displaced 20 Å closer and also 20 Å further from residue 22 (weighting of 1:2:1) resulted in a good fit to the data as shown in Figures 7A and 7B (yellow lines). For the same procedure but with the core displaced only $\pm 10 \text{ Å}$, the fit was still poor (Figure S3).

The results shown thus far were obtained after the adsorption process advanced to near completion. To gain insight into the kinetics of the process and how quickly Nef inserts and undergoes conformational change, the conformation of myr-dNef was also studied at early stages of adsorption by injecting myr-Nef at 0.67 μM underneath a monolayer of dDPPG at 20 mN/m and collecting successive scans over a limited q_z range during the adsorption process. The NR results given in Figures 8A and 8B reveal that at early stages of adsorption (coverages of $f = 0.07$, 0.23, and 0.37), membrane-bound myr-dNef was predominantly in the open form. The trough area continued to increase steadily during these scans (Figure 8C), indicating insertion of residues into the membrane.

Finally, the importance of the myristate group to the conformational change was examined by studying adsorption of nonmyristoylated Nef (nonmyr-Nef) to monolayers of dDPPG at 30 mN/m. In this case, a deuterated Nef construct containing a N-terminal His tag was used, as described previously (Kent et al., 2010). The dDPPG monolayer was spread to 16 mN/m and then compressed to 30 mN/m before introduction of nonmyr-Nef. For this construct of Nef lacking the myristate group, the affinity for the dDPPG membrane was substantially reduced compared to myr-Nef, and adsorption to relatively high coverage ($f = 0.21$) required 9 hr at 1 μM. The NR data and corresponding profiles (Figures S1A and S1B) of nonmyr-Nef indicated no insertion and no movement of the barrier (Figure S1C). The SLD profile is that of a compact form with the core domain against the lipid headgroups. Thus, in the absence of the myristate group, insertion of N-terminal arm residues and the transition to the open form do not occur. Comparison of these results for nonmyr-Nef with the results in Figure 2 for myr-Nef at the same conditions (1 μM Nef and dDPPG at 30 mN/m) demonstrates that insertion of the N-terminal arm and the transition to the open form is promoted by insertion of the myristate group.

DISCUSSION

Resolving the structure of membrane-associated proteins is extremely challenging yet critically important because positioning of residues and motifs relative to the membrane can strongly affect function. While important progress has been made recently (Chen et al., 2009; Datta et al., 2011; Kent et al., 2010; Krepkiy et al., 2012; McGillivray et al., 2009; Nanda et al., 2010; Shenoy et al., 2012), not much is known about the precise distribution of residues of membrane-associated proteins with respect to lipid membranes due to a lack of adequate tools and methods. The present NR and XR data have revealed that membrane-bound myr-Nef adopts a very different conformation depending upon the ability of residues to insert into the lipid membrane.

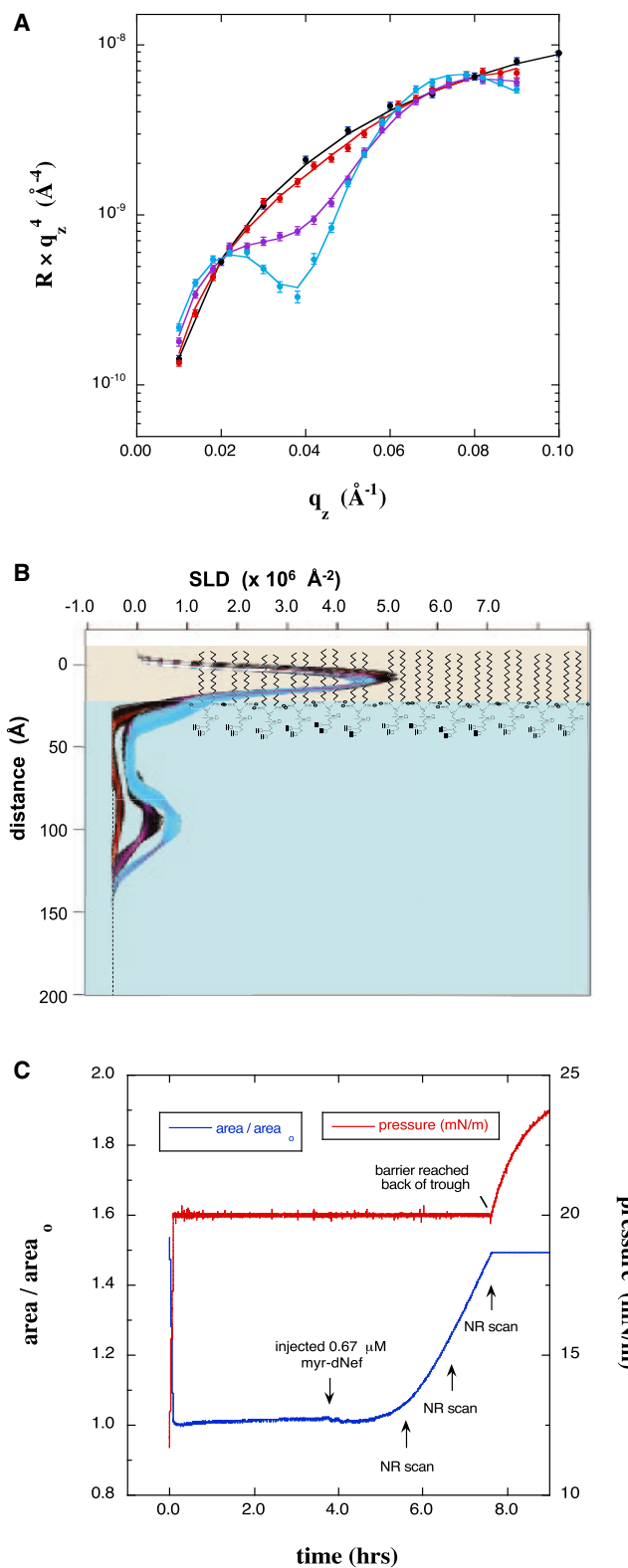


Figure 8. NR Results for myr-dNef Adsorbed at Different Coverages to a dDPPG Monolayer at 20 mN/m

(A) NR data for a dDPPG monolayer at 20 mN/m on Tris-buffered H_2O subphase (black) along with scans collected 2 hr (red), 3 hr (purple), and 4 hr

Our data are entirely consistent with previous hypotheses (Bentham et al., 2006; Curtain et al., 1998; Gerlach et al., 2010) that myr-Nef adsorbs through a combination of electrostatic interactions between basic residues in the N-terminal arm and the negatively charged lipid headgroups, followed by insertion of the hydrophobic myristate group and amphipathic helix. We observed a substantially lower binding affinity with decreasing fraction of negatively charged lipids or in absence of the myristate group, arguing that both lipid association and electrostatic attraction affect the ability of Nef to associate and insert.

Our results indicate that insertion of residues into the membrane is the key step initiating the transition to the open form. In the absence of insertion, here as a result of high membrane pressure, membrane-bound Nef adopts a closed form with the core domain directly against the lipid headgroups. At lower membrane pressure where the myristate and amino acid residues are readily able to insert into the membrane, Nef adopts an open form in which the core domain is displaced into solution $\sim 70 \text{\AA}$ from the lipid headgroups. From the extent of the increase in area, it is clear that a substantial number of residues, presumably residues 5–22 on the N-terminal arm known to form an amphipathic helix (Gerlach et al., 2010), insert in addition to the myristate group. Fitting the NR data with molecular models of Nef indicates that the 70\AA average distance of the core domain from the membrane in the open conformation is fully consistent with residues 5–22 residing within the lipid headgroup region. The data suggest that interactions between the N-terminal arm and the core domain that exist in solution are broken upon insertion of a portion of the N-terminal arm into the lipid monolayer, and that the latter is facilitated by the insertion of myristate group. The rate and extent of residue insertion are influenced by the density of adsorbed Nef, by the membrane pressure (lipid packing density), and by the presence of the N-terminal myristate. At a membrane pressure of 30 mN/m, insertion and the open form resulted only at higher myr-Nef concentration whereas at 20 mN/m, insertion and the open form resulted even at low myr-Nef concentration. Furthermore, at a membrane pressure of 30 mN/m and a concentration of 1 μM , insertion and the open form resulted for myr-Nef but not for Nef lacking the N-terminal myristate.

The open form is not triggered by high coverage of Nef on the membrane. Time-dependent scans collected at early stages of adsorption at 20 mN/m show that Nef is predominantly in the open form even at low coverages. Indeed, high coverage ($f = 0.37$) and yet very little insertion resulted in a prior study involving His-Nef adsorption to lipid monolayers containing a synthetic metal-chelating lipid (Kent et al., 2010), and in that case Nef remained in the closed form. The transition to the open form does not appear to be triggered by electrostatic repulsion of the core from the membrane because the open form was

(cyan) after injecting 0.67 μM myr-dNef. The minimum at $q_z = 0.04 \text{\AA}^{-1}$ is indicative of the thickness of the adsorbed protein layer.

(B) SLD profiles corresponding to the data in (A). Red, purple, and cyan profile bands correspond to 2 hr, 3 hr, and 4 hr after addition of myr-hNef, respectively. The profiles indicate that at the earliest stages of adsorption membrane-bound Nef is predominantly in the open form.

(C) Normalized trough area versus time showing the expansion of the area upon injection of myr-dNef and the time at which the NR scans were initiated.

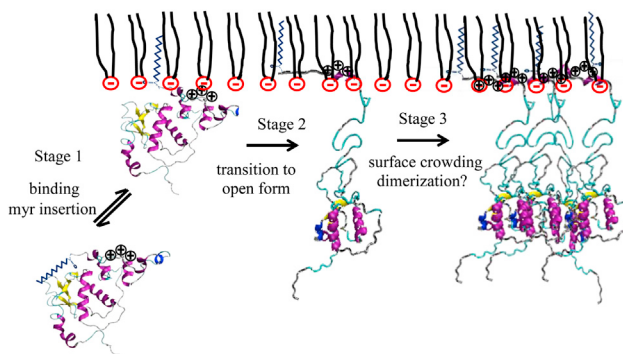


Figure 9. Mechanism of myr-Nef Binding to a dDPPG Membrane

Myr-Nef is adsorbed through electrostatic attraction and myristate insertion at the first stage. This is identical to the fast process observed by Gerlach et al., 2010. At higher surface pressures (35 mN/m), there is no change in the conformation of myr-Nef after the first stage. At lower pressures (20 mN/m) with the insertion of the N-terminal arm into the membrane (slow process of Gerlach and colleagues), the core domain is displaced 70 Å away from the membrane. Surface coverage of myr-Nef in open conformation increases very slowly as a function of time, perhaps involving membrane-driven dimerization (Poe and Smithgall, 2009). Stages 1 and 2 occur on timescales that are too fast to be detected by NR or XR.

obtained for membranes containing as little as 30% negatively charged lipids, and the displacement distance of the core domain from the lipid headgroups was nearly identical for 30% and 100% of negatively charged lipids. Furthermore, the open form did not result when insertion of residues was blocked by a high membrane pressure, despite a greater lipid packing density and therefore greater electrostatic repulsion than at lower membrane pressures.

Gerlach and colleagues reported a kinetic study of myr-Nef binding to fluid phase membranes of DOPC and DOPG using FRET (Gerlach et al., 2010). Strong myr-Nef binding required the presence of negatively charged lipids, as also observed in the present study. The kinetic data indicated two processes: a fast process that was attributed to electrostatic-driven association followed by myristate insertion, and a slower process that was attributed to insertion and formation of an amphipathic helix within the N-terminal 27 residues. They showed that the rate of the fast process increased with membrane curvature, consistent with more rapid insertion of myristate into more loosely packed lipids. This is analogous to and entirely consistent with this study in which surface pressure and packing density were used to alter the energy barrier for insertion.

While the kinetic study of Gerlach and colleagues revealed two processes, no information was provided on the conformation of Nef corresponding to those processes. The present study provides this insight. While both processes in the study of Gerlach and colleagues occurred on time scales much faster than can be resolved by NR and XR, by increasing the energetic barrier for residue insertion we isolated the membrane-bound conformation in absence of helix insertion. In that case, corresponding to the conformation at the end of the fast process of Gerlach and colleagues, Nef is in the closed form (Figure 9). The present data reveal that upon insertion of the amphipathic helix (the slow process of Gerlach and colleagues), Nef adopts an open conformation in which the core domain is displaced on average 70 Å from

the lipid headgroups. In addition to providing insight into the conformation of Nef during the processes elucidated by Gerlach and colleagues, the present data also reveal a much longer time scale process in which the coverage of open form Nef on the membrane increases (Figure 9). The present data thus inform the Gerlach model with respect to the conformations of Nef and also extend it to include a longer time scale process of increasing coverage.

It is interesting to speculate about how the present results may be tied to Nef biology and what role Nef insertion and conformation change may play in the ability of Nef to associate with binding partners that lead to Nef signaling/function. Recently, Jia and colleagues determined the crystal structure of a complex of Nef with the cytoplasmic domain of MHC-I using a construct in which the MHC-I cytoplasmic domain was fused to the N terminus of Nef (Jia et al., 2012). In the crystal structure, the N-terminal helix of Nef (residues 6–22) was attached to the core domain of Nef through interactions involving Trp13 and Met20. The authors speculated that this association persists upon membrane binding and positions the Nef core close to the membrane for optimal interaction with the cytoplasmic domain of the MHC-I receptor. The present data are at odds with the assertion that the N-terminal helix of Nef remains attached to the core domain upon membrane binding. Rather, our results show that the N-terminal arm inserts into lipid membranes and the core domain is displaced 70 Å from the membrane in absence of a binding partner protein. However, this fact is not in any way inconsistent with Nef interaction with the receptor, as each core domain is free to explore the full range of distance from the membrane. The 70 Å distance is the average of the distribution of displacements. Jia and colleagues reported that mutations W13A or M20A abolished Nef-induced downregulation of MHC-I in human T lymphocytes, and this was presented as further support for their assertion that interaction of Trp 13 and Met20 with the core domain of Nef is critical for the downregulation of MHC-I. However, these residues likely play important roles in membrane binding and insertion. Therefore, it is entirely possible that the effects of these mutations observed in T lymphocytes are due to decreased membrane association or altered insertion and helix formation.

The present data also provide strong evidence against the assertion (Horenkamp et al., 2011) that association of the core domain of Nef with negatively charged membranes through its basic surface (Figure 1B) orients Nef to provide optimal exposure of the dileucine sorting motif in the flexible loop (residues 152–184) known to mediate interactions with adaptor protein complexes. As we have shown, because the core domain is displaced 70 Å from the lipid membrane in its final resting position, it is unlikely that the membrane affects Nef orientation.

Extensive evidence indicates that at least some functions of Nef *in vivo* require dimerization (Poe and Smithgall, 2009), yet we (using glutaraldehyde crosslinking) and others (Breuer et al., 2006; Horenkamp et al., 2011) have found no evidence for dimerization of free Nef in solution at 1 μM. It was shown elsewhere using analytical gel filtration that in solution, truncated Nef lacking N-terminal residues 2–44 contains significant dimeric and multimeric fractions, whereas myr-Nef and nonmyr-Nef exist primarily as monomers (Breuer et al., 2006). This suggests that

Structure

Conformation of Membrane-Associated HIV-1 Nef

dimerization of Nef may be inhibited by association of the N-terminal arm with the core domain. Residues on α helix 4 and the adjacent loop (R109–D127) have been identified as promoting Nef dimer and trimer association (Lee et al., 1996; Arold et al., 1997). Others have proposed that membrane insertion of the myristate group causes the N-terminal arm to separate from the core domain and thereby promotes Nef dimerization (Arold and Baur, 2001; Geyer et al., 2001). Unfortunately, reflectivity methods are unable to detect structural changes that occur in the plane of the membrane; thus, our results do not directly inform the dimeric status of myr-Nef at the membrane. However, our results with NR and XR show that substantially higher coverages are ultimately achieved with Nef in the open form, and thus are consistent with the hypothesis that the arm must separate from the core of the protein to promote multimerization.

In summary, we report the measurement of the precise location of the core domain of terminally acylated Nef with respect to a lipid membrane. Hundreds of proteins are known to be lipidated, including many that are related to signaling and disease states, and many are potential targets for therapeutic intervention. The present approach will be useful to resolve the membrane-bound conformations of these proteins and will provide insights into signaling mechanisms. It can also inform on the effects of protein-protein interaction at the membrane and disruption of said interactions with pharmacological agents.

EXPERIMENTAL PROCEDURES

Materials

dDPPG and dDPPC in which the 62 protons in the aliphatic tails were replaced with deuterons were purchased from Avanti Polar Lipids. These deuterated lipids were used for both NR and XR measurements. Tris buffer salts and dithiothreitol (DTT) were purchased from Sigma-Aldrich and used as received.

Proteins

Protonated myristolated-Nef (myr-Nef) was expressed in *Escherichia coli* as described elsewhere (Morgan et al., 2011) using a pET-Duet-1 vector that contained both h-NMT-1 and SF2 Nef (with a C-terminal histidine purification tag). Expression was carried out in 1 l M9 minimal media until the optical density reached 0.6, supplemented afterward for 10 min with 10 ml of 5 mM myristic acid with 0.6 μ M BSA. Cells were induced with 1 mM IPTG overnight at 16°C. Purification was performed with Ni-NTA agarose, as described previously (Morgan et al., 2011) and the final purified species was >95% myristylated, as determined by mass spectrometry. Deuterated myr-Nef (myr-dNef) was prepared by expression in a modified M9 media made with 99.8% D₂O; deuterium incorporation was checked by mass spectrometry and showed that the protein was 80% deuterated (data not shown).

Methods

Adsorption Studies

The Langmuir trough and monolayer system are illustrated in Figure 1C. In a typical adsorption run, dDPPG was spread from a 70/30 (by vol.) mixture of chloroform and methanol on the surface of 20 mM Tris-buffered H₂O subphase (pH 8.2, 100 mM NaCl) held within the Teflon trough (70 mm × 70 mm × 2 mm; Figure 1C). After allowing the chloroform and methanol to evaporate, the surface layer was compressed to the final target pressure by a movable barrier. Sufficient lipid was deposited such that after reaching the target pressure, the barrier remained outside of the footprint of the neutron or X-ray beam (Figure 1C). After collecting NR or XR data for the lipid monolayer alone, myr-Nef was then injected into the subphase underneath the lipid monolayer. Successive reflectivity scans were then initiated until adsorption was completed. In some cases, the subphase was then exchanged with Tris buffer containing

1 mM DTT using a peristaltic pump and Teflon tubing with an inlet and outlet submerged at opposite ends of the trough. All tubing and fittings were made of Teflon and cleaned using water and Tris buffer after each experiment. The trough was maintained at 20°C ± 2°C.

Neutron and X-Ray Reflection

NR measurements were performed on the NG7 (NCNR/NIST) and Liquids (SNS/ORNL) reflectometers. Details of these spectrometers and the measurement protocols are given in the *Supplemental Experimental Procedures*. XR measurements were performed using an X-ray reflectometer (Bruker, D8 Advance) employing Cu K α radiation at NCNR/NIST (Gaithersburg, MD). The copper source was operated at 40 kV and 40 mA, and the wavelength was 0.154 nm. The beam width was 10 mm and the beam height was 0.1 mm.

The NR and XR data were analyzed using the Ga_refl program based on the optical matrix method. Ga_refl is available at <http://www.ncnr.nist.gov>. Simultaneous fits of the data were performed at different stages of a single adsorption run (for example lipids only, with adsorbed protein, and after subphase exchange). The SLD of the subphase was held constant for all the fits. Analyses were performed with free-form models involving a small number of slabs, as well as using molecular structures. The molecular structure of myr-Nef was generated from 1QA5 and 2NEF and manipulated in NAMD2 using the CHARMM22 force field. For fitting NR data, the free-form models consisted of one layer each for the lipid tails and the lipid headgroups, and one to four layers for the protein as required to achieve a good fit to the data. When no insertion occurred, as indicated by little or no movement of the barrier, the thickness and SLD of the lipid tail layer after adsorption of myr-dNef were constrained to the same values as determined for the data taken prior to adsorption. This is based on the XR results (Figure 4), where lack of change in thickness of the lipid layers is demonstrated by absence of a shift in the fringes. For the free-form fit to the NR data in Figure 7, the thickness of the lipid tail layer after insertion of myr-dNef was constrained to be 4 Å less than that measured for dDPPG alone, based on the XR results in Figure 3. Based on the relative areas occupied by the core domain of Nef and a DPPG molecule, and the fact that the myristate group has only a single aliphatic chain, the SLD of the lipid tail layer was constrained to be greater than or equal to $0.95 \times \text{SLD}_{\text{tails dDPPG}} + 0.05 \times \text{SLD}_{\text{myr}}$. For the fits to the data in Figure 7 involving molecular models of Nef, the number of Nef molecules per area and z-position of the core domain varied in the fits, in addition to the thickness and SLD of the lipid tails and headgroups layers. The SLD of the lipid tail layer was constrained to be equal to $(1.0 - 0.05 \times f) \times \text{SLD}_{\text{tails dDPPG}} + 0.05 \times f \times \text{SLD}_{\text{myr}}$ to account for insertion of the protonated myristate group. In the Ga_refl program, the roughness parameter is the full width at half maximum (FWHM = 2.35 σ , where σ is the standard deviation) of a Gaussian distribution and was constrained in the fitting to be less than the smallest thickness of the two adjacent layers.

Fitting reflectivity data results in defining a family of SLD curves that are consistent with the data. The uncertainty in the fitted profiles was determined by a Monte Carlo resampling procedure in which a large number (1,000) of statistically independent sets of reflectivity data were created from the original data set and the error bars from the counting statistics. The result is a range of values for each fit parameter that is consistent with the statistics of the original data. The uncertainty in a fitted profile is represented by a color-coded band (Figures 6, 7, and 8). This method has been reported in detail elsewhere (Heinrich et al., 2009). The analysis focuses on the location of structural motifs (N-terminal arm and core domain) relative to the membrane. The positions of individual atoms cannot be determined due to insufficient spatial resolution.

Nef coverages were obtained by first converting the SLD or electron density profiles to amino acid (aa) volume fraction profiles using $\text{SLD} = \phi_{\text{aa}}(\text{SLD}_{\text{aa}}) + (1 - \phi_{\text{aa}})(\text{SLD}_{\text{water}})$ or $\rho_e = \phi_{\text{aa}}(\rho_{e \text{ aa}}) + (1 - \phi_{\text{aa}})(\rho_{e \text{ water}})$, and then integrating the aa volume fraction profiles to obtain the volume (or mass) of Nef per unit area. A coverage of 1.0 was defined as the area per Nef molecule for the open form conformation shown in Figures 2 and 7. The average neutron SLD values (SLD_{aa}) for myr-Nef and myr-dNef (80% deuteration) are 2.02×10^{-6} Å⁻² and 5.19×10^{-6} Å⁻², respectively. The X-ray SLD is directly proportional to the electron density, where the constant of proportionality is the classical electron radius (2.82×10^{-5} Å). The calculated average electron density ($\rho_{e \text{ aa}}$) and X-ray SLD ($\lambda = 1.54$ Å) for myr-Nef are $0.426 \text{ e}/\text{\AA}^3$ and 1.201×10^{-5} Å⁻², respectively.

SUPPLEMENTAL INFORMATION

Supplemental Information includes Supplemental Experimental Procedures and three figures and can be found with this article online at <http://dx.doi.org/10.1016/j.str.2013.08.008>.

ACKNOWLEDGMENTS

Sandia is a multiprogram laboratory operated by Sandia Corporation, a Lockheed Martin Company, for the U.S. Department of Energy under contract DE-AC04-94AL85000. We acknowledge the support of the National Institute of Standards and Technology, the U.S. Department of Commerce, in providing the neutron research facilities used in this work. Research conducted at ORNL's Spallation Neutron Source was sponsored by the Scientific User Facilities Division, Office of Basic Energy Sciences, U.S. Department of Energy. This work was supported by NIH grant R01-GM086507 (to M.S.K. and J.R.E.) and R01-GM101647-02 (to H.N.). Commercial materials, instruments, and equipment are identified in this paper to specify the experimental procedure as completely as possible. In no case does such identification imply a recommendation or endorsement by the National Institute of Standards and Technology, nor does it imply that the materials, instruments, or equipment identified are necessarily the best available for the purpose.

Received: April 20, 2013

Revised: July 8, 2013

Accepted: August 2, 2013

Published: September 12, 2013

REFERENCES

- Ames, J.B., Tanaka, T., Stryer, L., and Ikura, M. (1996). Portrait of a myristoyl switch protein. *Curr. Opin. Struct. Biol.* 6, 432–438.
- Arold, S.T., and Baur, A.S. (2001). Dynamic Nef and Nef dynamics: how structure could explain the complex activities of this small HIV protein. *Trends Biochem. Sci.* 26, 356–363.
- Arold, S., Franken, P., Strub, M.P., Hoh, F., Benichou, S., Benarous, R., and Dumas, C. (1997). The crystal structure of HIV-1 Nef protein bound to the Fyn kinase SH3 domain suggests a role for this complex in altered T cell receptor signaling. *Structure* 5, 1361–1372.
- Baur, A. (2004). Functions of the HIV-1 Nef protein. *Curr. Drug Targets Immune Endocr. Metabol. Disord.* 4, 309–313.
- Bentham, M., Mazaleyrat, S., and Harris, M. (2006). Role of myristylation and N-terminal basic residues in membrane association of the human immunodeficiency virus type 1 Nef protein. *J. Gen. Virol.* 87, 563–571.
- Breuer, S., Gerlach, H., Kolaric, B., Urbanke, C., Opitz, N., and Geyer, M. (2006). Biochemical indication for myristylation-dependent conformational changes in HIV-1 Nef. *Biochemistry* 45, 2339–2349.
- Chen, C.-H., Máliková, S., Pingali, S.V., Long, F., Garde, S., Cho, W., and Schlossman, M.L. (2009). Configuration of PKC α -C2 domain bound to mixed SOPC/SOPS lipid monolayers. *Biophys. J.* 97, 2794–2802.
- Coates, K., Cooke, S.J., Mann, D.A., and Harris, M.P. (1997). Protein kinase C-mediated phosphorylation of HIV-I nef in human cell lines. *J. Biol. Chem.* 272, 12289–12294.
- Curtain, C.C., Lowe, M.G., Macreadie, I.G., Gentle, I.R., Lawrie, G.A., and Azad, A.A. (1998). Structural requirements for the cytotoxicity of the N-terminal region of HIV type 1 Nef. *AIDS Res. Hum. Retroviruses* 14, 1543–1551.
- Das, S.R., and Jameel, S. (2005). Biology of the HIV Nef protein. *Indian J. Med. Res.* 121, 315–332.
- Datta, S.A.K., Heinrich, F., Raghunandan, S., Krueger, S., Curtis, J.E., Rein, A., and Nanda, H. (2011). HIV-1 Gag extension: conformational changes require simultaneous interaction with membrane and nucleic acid. *J. Mol. Biol.* 406, 205–214.
- Farazi, T.A., Waksman, G., and Gordon, J.I. (2001). The biology and enzymology of protein N-myristylation. *J. Biol. Chem.* 276, 39501–39504.
- Flaherty, K.M., Zozulya, S., Stryer, L., and McKay, D.B. (1993). Three-dimensional structure of recoverin, a calcium sensor in vision. *Cell* 75, 709–716.
- Gerlach, H., Laumann, V., Martens, S., Becker, C.F.W., Goody, R.S., and Geyer, M. (2010). HIV-1 Nef membrane association depends on charge, curvature, composition and sequence. *Nat. Chem. Biol.* 6, 46–53.
- Geyer, M., and Peterlin, B.M. (2001). Domain assembly, surface accessibility and sequence conservation in full length HIV-1 Nef. *FEBS Lett.* 496, 91–95.
- Geyer, M., Munte, C.E., Schorr, J., Kellner, R., and Kalbitzer, H.R. (1999). Structure of the anchor-domain of myristylated and non-myristylated HIV-1 Nef protein. *J. Mol. Biol.* 289, 123–138.
- Geyer, M., Fackler, O.T., and Peterlin, B.M. (2001). Structure–function relationships in HIV-1 Nef. *EMBO Rep.* 2, 580–585.
- Goldberg, J. (1998). Structural basis for activation of ARF GTPase: mechanisms of guanine nucleotide exchange and GTP-myristoyl switching. *Cell* 95, 237–248.
- Goldsmith, M.A., Warmerdam, M.T., Atchison, R.E., Miller, M.D., and Greene, W.C. (1995). Dissociation of the CD4 downregulation and viral infectivity enhancement functions of human immunodeficiency virus type 1 Nef. *J. Virol.* 69, 4112–4121.
- Grzesiek, S., Bax, A., Clore, G.M., Gronenborn, A.M., Hu, J.-S., Kaufman, J., Palmer, I., Stahl, S.J., and Wingfield, P.T. (1996). The solution structure of HIV-1 Nef reveals an unexpected fold and permits delineation of the binding surface for the SH3 domain of Hck tyrosine protein kinase. *Nat. Struct. Biol.* 3, 340–345.
- Grzesiek, S., Bax, A., Hu, J.S., Kaufman, J., Palmer, I., Stahl, S.J., Tjandra, N., and Wingfield, P.T. (1997). Refined solution structure and backbone dynamics of HIV-1 Nef. *Protein Sci.* 6, 1248–1263.
- Hanna, Z., Priceputu, E., Kay, D.G., Poudrier, J., Chrobak, P., and Jolicœur, P. (2004). In vivo mutational analysis of the N-terminal region of HIV-1 Nef reveals critical motifs for the development of an AIDS-like disease in CD4C/HIV transgenic mice. *Virology* 327, 273–286.
- Hantschel, O., Nagar, B., Guettler, S., Kretzschmar, J., Dorey, K., Kuriyan, J., and Superti-Furga, G. (2003). A myristoyl/phosphotyrosine switch regulates c-Abl. *Cell* 112, 845–857.
- Harris, M. (1995). The role of myristylation in the interactions between human immunodeficiency virus type I Nef and cellular proteins. *Biochem. Soc. Trans.* 23, 557–561.
- Heinrich, F., Ng, T., Vanderah, D.J., Shekhar, P., Mihailescu, M., Nanda, H., and Lösche, M. (2009). A new lipid anchor for sparsely tethered bilayer lipid membranes. *Langmuir* 25, 4219–4229.
- Horenkamp, F.A., Breuer, S., Schulte, A., Lülf, S., Weyand, M., Saksela, K., and Geyer, M. (2011). Conformation of the dileucine-based sorting motif in HIV-1 Nef revealed by intermolecular domain assembly. *Traffic* 12, 867–877.
- Jeromin, A., Muralidhar, D., Parameswaran, M.N., Roder, J., Fairwell, T., Scarlata, S., Dowal, L., Mustafi, S.M., Chary, K.V., and Sharma, Y. (2004). N-terminal myristylation regulates calcium-induced conformational changes in neuronal calcium sensor-1. *J. Biol. Chem.* 279, 27158–27167.
- Jia, X., Singh, R., Homann, S., Yang, H., Guatelli, J., and Xiong, Y. (2012). Structural basis of evasion of cellular adaptive immunity by HIV-1 Nef. *Nat. Struct. Mol. Biol.* 19, 701–706.
- Jung, J.J., Byeon, I.-J.L., Ahn, J., and Gronenborn, A.M. (2011). Structure, dynamics, and Hck Interaction of full-length HIV-1 Nef. *Proteins: Structure, Function, and Bioinformatics* 79, 1609–1622.
- Kent, M.S., Murton, J.K., Sasaki, D.Y., Satija, S., Akgun, B., Nanda, H., Curtis, J.E., Majewski, J., Morgan, C.R., and Engen, J.R. (2010). Neutron reflectometry study of the conformation of HIV Nef bound to lipid membranes. *Biophys. J.* 99, 1940–1948.
- Kim, L.C., Song, L., and Haura, E.B. (2009). Src kinases as therapeutic targets for cancer. *Nat Rev Clin Oncol* 6, 587–595.
- Klotman, M.E., Kim, S., Buchbinder, A., DeRossi, A., Baltimore, D., and Wong-Staal, F. (1991). Kinetics of expression of multiply spliced RNA in early human immunodeficiency virus type 1 infection of lymphocytes and monocytes. *Proc. Natl. Acad. Sci. USA* 88, 5011–5015.

- Krepkiy, D., Gawrisch, K., and Swartz, K.J. (2012). Structural interactions between lipids, water and S1-S4 voltage-sensing domains. *J. Mol. Biol.* 423, 632–647.
- Lee, C.-H., Saksela, K., Mirza, U.A., Chait, B.T., and Kuriyan, J. (1996). Crystal structure of the conserved core of HIV-1 Nef complexed with a Src family SH3 domain. *Cell* 85, 931–942.
- Matsubara, M., Nakatsu, T., Kato, H., and Taniguchi, H. (2004). Crystal structure of a myristoylated CAP-23/NAP-22 N-terminal domain complexed with Ca²⁺/calmodulin. *EMBO J.* 23, 712–718.
- McGillivray, D.J., Valinicius, G., Heinrich, F., Robertson, J.W.F., Vanderah, D.J., Febo-Ayala, W., Ignatjev, I., Lösche, M., and Kasianowicz, J.J. (2009). Structure of functional *Staphylococcus aureus* alpha-hemolysin channels in tethered bilayer lipid membranes. *Biophys. J.* 96, 1547–1553.
- McLaughlin, S., and Aderem, A. (1995). The myristoyl-electrostatic switch: a modulator of reversible protein-membrane interactions. *Trends Biochem. Sci.* 20, 272–276.
- Morgan, C.R., Miglionico, B.V., and Engen, J.R. (2011). The effects of HIV-1 Nef on human N-myristoyl transferase 1. *Biochemistry* 50, 3394–3403.
- Nanda, H., Datta, S.A.K., Heinrich, F., Lösche, M., Rein, A., Krueger, S., and Curtis, J.E. (2010). Electrostatic interactions and binding orientation of HIV-1 matrix studied by neutron reflectivity. *Biophys. J.* 99, 2516–2524.
- Narute, P.S., and Smithgall, T.E. (2012). Nef alleles from all major HIV-1 clades activate Src-family kinases and enhance HIV-1 replication in an inhibitor-sensitive manner. *PLoS ONE* 7, e32561.
- Osterhout, J.L., Waheed, A.A., Hiol, A., Ward, R.J., Davey, P.C., Nini, L., Wang, J., Milligan, G., Jones, T.L.Z., and Druey, K.M. (2003). Palmitoylation regulates regulator of G-protein signaling (RGS) 16 function. II. Palmitoylation of a cysteine residue in the RGS box is critical for RGS16 GTPase accelerating activity and regulation of Gi-coupled signalling. *J. Biol. Chem.* 278, 19309–19316.
- Penfold, J., and Thomas, R. (1990). The application of the specular reflection of neutrons to the study of surfaces and interfaces. *J. Phys. Condens. Matter* 2, 1369–1412.
- Peng, B., and Robert-Guroff, M. (2001). Deletion of N-terminal myristylation site of HIV Nef abrogates both MHC-1 and CD4 down-regulation. *Immunol. Lett.* 78, 195–200.
- Perinpanayagam, M.A., Beauchamp, E., Martin, D.D.O., Sim, J.Y.W., Yap, M.C., and Berthiaume, L.G. (2013). Regulation of co- and post-translational myristylation of proteins during apoptosis: interplay of N-myristoyltransferases and caspases. *FASEB J.* 27, 811–821.
- Poe, J.A., and Smithgall, T.E. (2009). HIV-1 Nef dimerization is required for Nef-mediated receptor downregulation and viral replication. *J. Mol. Biol.* 394, 329–342.
- Raney, A., Shaw, A.Y., Foster, J.L., and Garcia, J.V. (2007). Structural constraints on human immunodeficiency virus type 1 Nef function. *Virology* 368, 7–16.
- Renkema, G.H., and Saksela, K. (2000). Interactions of HIV-1 NEF with cellular signal transducing proteins. *Front. Biosci.* 5, D268–D283.
- Resh, M.D. (2006). Trafficking and signaling by fatty-acylated and prenylated proteins. *Nat. Chem. Biol.* 2, 584–590.
- Schlessinger, J. (2000). Cell signaling by receptor tyrosine kinases. *Cell* 103, 211–225.
- Shenoy, S.S., Nanda, H., and Lösche, M. (2012). Membrane association of the PTEN tumor suppressor: Electrostatic interaction with phosphatidylserine-containing bilayers and regulatory role of the C-terminal tail. *J. Struct. Biol.* 180, 394–408.
- Steinhauer, J., and Treisman, J.E. (2009). Lipid-modified morphogens: functions of fats. *Curr. Opin. Genet. Dev.* 19, 308–314.
- Subramanian, K., Dietrich, L.E.P., Hou, H., LaGrassa, T.J., Meiringer, C.T.A., and Ungermann, C. (2006). Palmitoylation determines the function of Vac8 at the yeast vacuole. *J. Cell Sci.* 119, 2477–2485.
- Welker, R., Harris, M., Cardel, B., and Kräusslich, H.G. (1998). Virion incorporation of human immunodeficiency virus type 1 Nef is mediated by a bipartite membrane-targeting signal: analysis of its role in enhancement of viral infectivity. *J. Virol.* 72, 8833–8840.
- Xue, L., Gollapalli, D.R., Maiti, P., Jahng, W.J., and Rando, R.R. (2004). A palmitoylation switch mechanism in the regulation of the visual cycle. *Cell* 117, 761–771.
- Zha, J., Weiler, S., Oh, K.J., Wei, M.C., and Korsmeyer, S.J. (2000). Posttranslational N-myristylation of BID as a molecular switch for targeting mitochondria and apoptosis. *Science* 290, 1761–1765.